

# Chronic Murine Typhoid Fever Is a Natural Model of Secondary Hemophagocytic Lymphohistiocytosis

Diane E. Brown<sup>1,2\*</sup>, Melissa W. McCoy<sup>1</sup>, M. Carolina Pilonieta<sup>1</sup>, Rebecca N. Nix<sup>1‡</sup>, Corrella S. Detweiler<sup>1\*</sup>

**1** Department of Molecular, Cellular and Developmental Biology, University of Colorado, Boulder, Colorado, United States of America, **2** Paleontology Section, Museum of Natural History, University of Colorado, Boulder, Colorado, United States of America

## Abstract

Hemophagocytic lymphohistiocytosis (HLH) is a hyper-inflammatory clinical syndrome associated with neoplastic disorders especially lymphoma, autoimmune conditions, and infectious agents including bacteria, viruses, protozoa and fungi. In both human and veterinary medicine, hemophagocytic histiocytic disorders are clinically important and frequently fatal. HLH in humans can be a primary (familial, autosomal recessive) or secondary (acquired) condition, with both types generally precipitated by an infectious agent. Previously, no mouse model for secondary HLH has been reported. Using *Salmonella enterica* serotype Typhimurium by oral gavage to mimic naturally-occurring infection in Sv129S6 mice, we characterized the clinical, hematologic and morphologic host responses to disease thereby describing an animal model with the clinicopathologic features of secondary HLH as set forth by the Histiocyte Society: fever, splenomegaly, cytopenias (anemia, thrombocytopenia), hemophagocytosis in bone marrow and spleen, hyperferritinemia, and hypofibrinogenemia. Disease severity correlates with high splenic and hepatic bacterial load, and we show disease course can be monitored and tracked in live animals. Whereby secondary HLH is known to occur in human patients with typhoid fever and other infectious diseases, our characterization of a viable natural disease model of secondary HLH offers an important means to elucidate pathogenesis of poorly understood mechanisms of secondary HLH and investigation of novel therapies. We characterize previously unreported secondary HLH in a chronic mouse model of typhoid fever, and novel changes in hematology including decreased tissue ferric iron storage that differs from classically described anemia of chronic disease. Our studies demonstrate *S. Typhimurium* infection of mice is a natural infectious disease model of secondary HLH that may have utility for elucidating disease pathogenesis and developing novel therapies.

**Citation:** Brown DE, McCoy MW, Pilonieta MC, Nix RN, Detweiler CS (2010) Chronic Murine Typhoid Fever Is a Natural Model of Secondary Hemophagocytic Lymphohistiocytosis. PLoS ONE 5(2): e9441. doi:10.1371/journal.pone.0009441

**Editor:** Stefan Bereswill, Charité-Universitätsmedizin Berlin, Germany

**Received:** January 31, 2010; **Accepted:** February 9, 2010; **Published:** February 26, 2010

**Copyright:** © 2010 Brown et al. This is an open-access article distributed under the terms of the Creative Commons Attribution License, which permits unrestricted use, distribution, and reproduction in any medium, provided the original author and source are credited.

**Funding:** This work was supported by grants AI076682 and AI072492 (C.S.D.) from the National Institutes of Health (www3.niaid.nih.gov). The funders had no role in study design, data collection and analysis, decision to publish, or preparation of the manuscript.

**Competing Interests:** The authors have declared that no competing interests exist.

\* E-mail: diane.brown@colorado.edu (DEB); corrella.detweiler@colorado.edu (CSD)

‡ Current address: Supergen, Salt Lake City, Utah, United States of America

## Introduction

Hemophagocytic lymphohistiocytosis (HLH), an inflammatory syndrome characterized by over-activation of macrophages and T lymphocytes, can be triggered by diverse eukaryotic, bacterial (especially intracellular), and viral pathogens [1–5]. HLH mortality rates can reach 50–90% in part due to late recognition and delayed onset of treatment [1,4]. Patients with clinicopathological characteristics of HLH are given differential diagnoses that include Macrophage Activation Syndrome, Hemophagocytic Histiocytosis, and Hemophagocytic Syndrome. The Histiocyte Society has endeavored to improve clinical recognition and resolve nomenclature issues by establishing a standard for HLH diagnostic criteria [5]. Veterinary literature has reflected similarly variable nomenclature for animals with hemophagocytic histiocytic disorders [6–10]. Regardless of primary diagnosis, the 2004 HLH diagnostic criteria require a patient have five of eight characteristics: hemophagocytic macrophages in bone marrow, spleen, and/or lymph nodes; two of three cytopenias (anemia, neutropenia, and/or thrombocytopenia); splenomegaly; hyperferritinemia; hypertriglyceridemia and/or hypofibrinogenemia; fever; high soluble CD25; and low natural killer (NK) cell activity [5].

HLH can be primary (familial, fHLH) or secondary (sHLH). Familial HLH is autosomal recessive, typically diagnosed in infants or children, fatal if untreated [2,4], and generally precipitated by infectious disease [3,5,11]. Thirty to seventy percent of fHLH cases are associated with genetic mutations that cause NK and/or CD8<sup>+</sup> T cell defects [5]. Four fHLH mouse models have been described [12–15]; three have spontaneous or genetically engineered mutations in *Pgf1*, *Unc13d* or *Rab27a*, and fHLH is triggered by viral infection. A fourth model is in mice deficient for asparaginyl endopeptidase (AEP, legumain) [15]. In summary, current mouse models of HLH involve genetic lesions and are models of fHLH.

Secondary HLH occurs in all age groups and is associated with infections across classes, malignancies especially lymphoma [1,3], and autoimmune disorders, absent any known underlying genetic defect [2]. HLH often has a nonspecific clinical presentation, and although pathophysiologically distinct, is difficult to clinically differentiate from sepsis [1,2,16], underlining the clinical importance of the Histiocyte Society's diagnostic criteria [5]. Difficulty in quantifying prevalence of sHLH is partly due to the diversity of underlying primary diseases, and evidence suggests it is likely under-diagnosed [2,4,17]. A fatality rate of 40% is reported for

sHLH cases without appropriate immuno-modulatory therapy [4]. Standardized diagnostic criteria should continue to improve recognition and yield more accurate prevalence statistics [5]. There are no reported mouse models of sHLH.

Data herein demonstrate that *Salmonella enterica* serotype Typhimurium (*S. Typhimurium*)-infected mice have clinico-pathological features of sHLH. Laboratory mice infected with *S. Typhimurium* model human typhoid fever which is caused by *Salmonella enterica* serovars Typhi and Paratyphi A, B and C [18]. Bacteria establish a chronic systemic infection in macrophages of Peyer's patches, mesenteric lymph nodes (MLN), spleen, liver and gall bladder [19–21]. Much of *S. Typhimurium* research has focused on fatal acute infections in mice compromised for innate immunity, generally Balb/c, C57BL/6, or DBA/1 strains, which are *Slc11a1/Nramp1*<sup>-/-</sup> [22,23]. However, in immunocompetent mice (*Sv129S6*, *Slc11a1/Nramp1*<sup>+/+</sup>) *S. Typhimurium* causes persistent systemic infection that most mice survive [19]. Both murine and human typhoid fever can result in a subclinical chronic carrier state [18,21]. Bacteria are found within macrophages during both acute and chronic infection [19,24,25], and cytokines including IL-1β and IL-18 are produced during pro-inflammatory caspase-1 dependent programmed cell death (pyroptosis) [26]. Hemophagocytic macrophages are a feature of both human typhoid fever [27–30] and HLH [5]. Importantly, *S. Typhimurium* replicates preferentially within cultured hemophagocytic macrophages in the *Sv129S6* mouse model [24]. Here we demonstrate that *Sv129S6* mice infected with *S. Typhimurium* acquire the clinico-pathological characteristics of HLH (Table 1), thus establishing an animal model for sHLH.

**Results**

Our findings of neurological disease, splenomegaly and inflammatory lesions are consistent with prior descriptions of murine *S. Typhimurium* infection [18,19,24,25,31–33,21]. Additionally, we describe detailed hematopoietic responses over the course of infection that characterize a) a non-lethal method to monitor *S. Typhimurium* infection via complete blood count (CBC), b) features of a secondary HLH syndrome, and c) responsive hematopoiesis with alterations in body iron that differ from anemia of inflammatory (or chronic) disease (ACD). Hematology and clinico-pathologic findings in *S. Typhimurium*-infected *Sv129S6* mice are summarized in Figure 1 (16-week study), and Tables 1 and 2 (10-week study).

**Clinical and Hematological Findings**

**Fever and neuropathy.** Infected mice developed slight fevers and clinical neurological signs including ataxia, head tilt, uni-directional circling when ambulating, and uni-directional rotatory spinning when lifted by the tail in seven of twenty-one mice (Table 1), and two of eight mice (16-week study). Mice with the most severe neurological signs failed to gain weight and accounted for the single early death in each study. While only fever is a formalized diagnostic criterion for HLH, both fever and neurological disease are common to HLH [1,3,2,34].

**Inflammatory leukogram.** Hematological findings included acute and ongoing response to infection characterized by immediate onset of neutrophilia (Figure 1A; Table 2) and later onset (3–5 weeks post-infection) of monocytosis (Figure 1B; Table 2). Rare band neutrophils were also seen. Lymphopenia (Figure 1C;

**Table 1.** Clinico-pathologic features of HLH in *S. Typhimurium*-infected mice.

	One-week PI	Three-weeks PI	Six-weeks PI	Ten-weeks PI
‡Increased hemophagocytic macrophages (bone marrow and/or spleen)	5/6 mice	4/6 mice	6/7 mice	2/2 mice
‡Fever		Days 17–23*		
‡Splenomegaly, % of body weight: median (range), fold difference from C	2X* (2-3X) 6/6 mice	3X (1-14X) 5/6 mice; 10/10 mice†	3X* (1-5X) 6/7 mice	3X (1-3X) 1/2 mice
‡Cytopenias:				
thrombocytopenia C range = 9.2–10.5×10 <sup>5</sup> /μL	2/6 mice (7.7–11.1)	5/6 mice* (0.9–9.8)	3/6 mice* (5.0–9.3)	0/2 mice (10.6–10.7)
anemia C range = 53–55 (HCT%)	1/6 mice* (48–53)	2/6 mice (29–53)	0/6 mice (51–56)	0/2 mice (51–55)
‡Hypofibrinogenemia C range (200–400 mg/dl)	0/6 mice	2/6 mice (100)	2/6 mice (100)	0/6 mice
‡Hyperferritinemia C range (699–1260 μg/L)	No	2/6 mice; 3/10 mice† (1425–6140)	No	No
Range CFU/g: spleen	10 <sup>2</sup> –10 <sup>4</sup>	10 <sup>4</sup> –10 <sup>5</sup>	10 <sup>3</sup> –10 <sup>4</sup>	10 <sup>1</sup> –10 <sup>2</sup>
liver	10 <sup>2</sup> –10 <sup>4</sup>	10 <sup>3</sup> –10 <sup>4</sup>	10 <sup>2</sup> –10 <sup>3</sup>	None detected
§Clinical neurological signs	7/21 mice- onset Day 5–12	6/21 mice – signs gone by Day 18	1/21 mice- early death Day 37	None
¶Chronic active hepatitis	Acute hepatitis 5/6 mice	Chronic active hepatitis 5/6 mice	Chronic active hepatitis 7/7 mice	Chronic active hepatitis 1/2 mice

PI indicates post-oral infection with 2.0×10<sup>9</sup> CFU *Salmonella enterica* serotype Typhimurium; C indicates mock-infected control mice.

\*P<0.05, Student's t-Test.

†Independent experiment, same bacterial dosing and range for splenic bacterial CFU results.

‡Formal diagnostic criteria for HLH per the Histiocyte Society guidelines [5].

§Consistent with a diagnosis of HLH, and ¶ strong supportive evidence for HLH [5].

doi:10.1371/journal.pone.0009441.t001

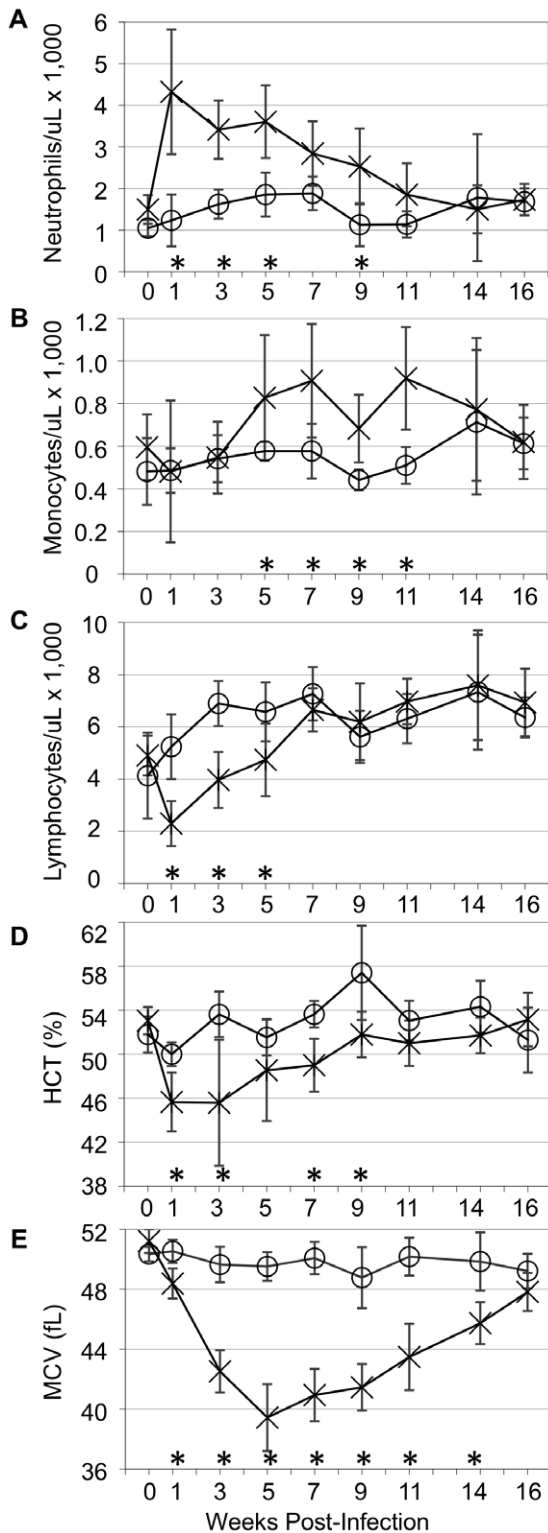


**Figure 1. Hematology of *S. Typhimurium*-infected mice: acute, then chronic active inflammatory response; microcytic anemia, persistent microcytosis.** Mice were orally gavaged with  $9.1 \times 10^8$  CFU of *S. Typhimurium* (n=8) or sterile PBS (n=7). Complete blood counts were monitored over 16 weeks. X = *S. Typhimurium*-infected mice; circle = mock-infected control mice. Mean and standard deviation are shown. (A) neutrophils, (B) monocytes, (C) lymphocytes, (D) hematocrit (HCT), (E) mean cell volume (MCV). \* $P < 0.05$  (Student's *t*-test). doi:10.1371/journal.pone.0009441.g001

Table 2) was consistent with a stress response from inflammatory disease and/or tissue infiltration by lymphocytes [1,35]. Up to 30% of lymphocytes had vacuolated cytoplasm. Thus, an acute inflammatory response transitioning to chronic active inflammation was demonstrated.

**Responsive microcytic anemia.** Infected mice had early onset slight to moderate microcytic anemia which was most severe at three weeks post-infection, correlating with highest bacterial tissue loads and most severe splenomegaly (Figure 1D–E; Table 2). Even after hematocrits (HCT) had recovered, microcytosis of erythrocytes (Figures 1D–E; Table 2) and reticulocytes (Table 2) persisted (demonstrated as decreased mean cell volume, MCV and MCVR, respectively). A marked regenerative erythroid response, measured by increased reticulocyte counts, polychromasia (Tables 1–2; Figure 2F) and red cell distribution widths (RDW) (Table 2), was present in highly infected mice. Reticulocytes were hypochromic (decreased CHR) at all time points (Table 2). These changes occurred together with hypoferrremia in all but one infected mouse at three weeks post-infection; this mouse had an appropriate macrocytic regenerative response consistent with its normal serum iron concentration (Table 2). Erythrocytosis, which can occur with microcytic anemia [36,37], was present from weeks 6–10 (Table 2, 10-week study), and 5–14 ( $P < 0.05$ ; 16-week study). Increased RDW at week six (Table 2) and weeks 3–14 ( $P < 0.05$ ; 16-week study) demonstrated erythrocyte anisocytosis. Blood film review confirmed erythrocyte anisocytosis, microcytosis and polychromasia (Figure 2E–F). Marked fragmentation (schistocytes) of mature and polychromatophilic erythrocytes (10–12% of cells affected) occurred at three weeks in highly infected mice (Figure 2F). Schistocytes were rare (~1%) at six weeks, and absent at 10 weeks post-infection. These data represent regenerative microcytic anemia and altered body iron status in highly infected mice.

**Thrombocytopenia.** Thrombocytopenia present from weeks 1–10 (Tables 1, 2) was most severe in highly infected mice at three weeks post-infection. Increased mean platelet volume (MPV) (Table 2) indicated increased thrombopoiesis in response to thrombocytopenia [35], and circulating macro-platelets were confirmed by blood film review; increased MPV was also present at weeks 1–11 ( $P < 0.05$ ) in the 16-week study (data not shown). Thus, *S. Typhimurium* infection in live animals can be monitored by CBC, and bi-cytopenia (anemia and thrombocytopenia), characteristic for HLH [5], was demonstrated in highly infected mice.

**Bacterial Tissue Loads and Splenomegaly**

Serum IgG titers to *Salmonella* O-Antigen, measured in the 16-week study, were 100–1,000 fold higher than mock-infected control from weeks 5–16 post-infection (data not shown). At 16-weeks post-infection, there was no recoverable *S. Typhimurium* in cecum, MLN, liver or spleen in five of eight mice, including two of five mice with high serum IgG. In the 10-week experiment (Table 1), bacterial colony forming units per gram (CFU/g) of liver and spleen was greatest at three weeks post-infection, consistent with the time-point of most severe HLH pathology (Tables 1–2), and decreased by six and 10 weeks post-infection.

Splenomegaly was present in six of seven infected mice at the conclusion of the 16-week study ( $P < 0.05$ ). Hepatosplenomegaly occurred at all time points in *S. Typhimurium*-infected mice in the 10-week study (Table 1). By comparison, livers of infected mice were 1.2 to 1.6 fold larger (median weight compared to body weight) than mock-infected controls overall ( $P < 0.05$  at one and three weeks post-infection). Mice with the highest splenic bacterial loads ( $10^5$  CFU/g at three weeks post-infection) had the largest

**Table 2.** Hematologic parameters of *S. Typhimurium*-infected mice.

Parameter	Week 1		Week 3		Week 6		Week 10	
	C, n=4	I, n=6	C, n=4	I, n=6	C, n=3	I, n=6	C, n=1	I, n=2
WBC × 10 <sup>3</sup> /μl	5.73 ± 1.61	5.32 ± 1.82	7.23 ± 1.93	5.32 ± 2.01	7.03 ± 1.62	8.13 ± 1.99	6.8	14.8, 6.7
RBC × 10 <sup>6</sup> /μl	9.79 ± 0.37	9.70 ± 0.25	9.79 ± 0.31	9.20 ± 1.83	9.64 ± 0.32	11.42* ± 0.25	8.86	11.43, 9.42
Neutrophils x10 <sup>3</sup> /μl	0.50 ± 0.20	1.35* ± 0.61	0.75 ± 0.21	1.25* ± 0.43	0.63 ± 0.23	1.82* ± 0.63	0.40	4.00, 0.60
Monocytes x10 <sup>3</sup> /μl	0.07 ± 0.06	0.17 ± 0.10	0.10 ± 0	0.23* ± 0.05	0.10 ± 0	0.43* ± 0.10	0.10	0.50, 0.10
Lymphocytes x10 <sup>3</sup> /μl	4.73 ± 1.34	3.57 ± 1.84	6.28 ± 1.37	3.72 ± 2.24	6.00 ± 1.68	5.70 ± 2.02	6.10	10.10, 5.80
HCT, %	53 ± 0.6	51* ± 1.6	53 ± 1.7	46 ± 11.3	53 ± 1.2	54 ± 1.8	51	55, 51
MCV, fl	54.0 ± 2.0	52.0 ± 0.9	54.3 ± 1.3	49.7 ± 4.8	55.7 ± 1.5	47.3* ± 1.0	58.0	48.0, 54.0
MCVr, fl	59.3 ± 1.5	56.3 ± 3.1	59.3 ± 0.5	52.8* ± 5.4	62.0 ± 1.0	55.8* ± 1.7	62.0	59.0, 63.0
MCHC, g/dl	31.0 ± 0	31.5 ± 0.5	31.3 ± 0.5	30.0 ± 1.8	30.0 ± 1.0	30.0 ± 0.6	30.0	30.0, 31.0
RDW	12.4 ± 0.4	12.7 ± 0.2	12.5 ± 0.2	16.7 ± 4.9	12.7 ± 0.1	14.6* ± 1.5	12.6	14.3, 13.0
Platelets x10 <sup>6</sup> /μl	1.02 ± 0.03	1.00 ± 0.14	0.92 ± 0.06	0.54* ± 0.33	1.05 ± 0.06	0.79* ± 0.16	0.87	1.06, 1.07
MPV, fl	7.3 ± 0.3	7.1 ± 0.2	7.3 ± 0.3	7.2 ± 1.0	7.7 ± 0.2	8.2 ± 0.6	6.7	7.1, 6.7
Reticulocytes x10 <sup>6</sup> /μl	0.48 ± 0.07	0.41 ± 0.18	0.40 ± 0.07	0.71 ± 0.40	0.44 ± 0.03	0.41 ± 0.06	0.57	0.54, 0.64
CHr, pg	17.9 ± 0.4	16.7* ± 1.0	17.7 ± 0.1	15.0* ± 2.3	17.4 ± 0.2	15.5* ± 0.4	17.4	15.8, 17.8
Serum Iron μg/dl	262 ± 10	297 ± 124	267 ± 26	219 ± 89	269 ± 30	266 ± 40	222	202, 280

Twenty-one mice were orally gavaged with 2.0 × 10<sup>9</sup> CFU of *S. Typhimurium* (I) and 13 mice with sterile PBS as mock-infected controls (C). No hematological data were obtained from one early death mouse. Complete blood counts (CBC) and serum iron were measured at weeks 1, 3, 6, and 10 post-infection. Data presented as mean ± 1 standard deviation, except 10 weeks where data from all mice shown.

WBC indicates white blood cells; RBC, red blood cells; HCT, hematocrit; MCV, mean cell volume; MCVr, mean cell volume reticulocytes; MCHC, mean cell hemoglobin concentration; RDW, red cell distribution width; MPV, mean platelet volume; and CHr, mean cell hemoglobin reticulocytes.

\*P < 0.05, Student's t-Test.

doi:10.1371/journal.pone.0009441.t002

spleens, and also the highest liver tissue loads (>5 × 10<sup>4</sup> CFU/g) and largest livers. An inverse correlation occurred between spleen weight, and HCT and platelet counts; infected mice with the greatest degree of splenomegaly had the lowest HCT and platelet counts. Importantly, splenomegaly persisted beyond the presence of measurable CFU of *S. Typhimurium*, and splenic bacterial load and splenomegaly correlated with the most severe cytopenias.

### Bone Marrow Cytopathology, Tissue Histopathology and Iron Studies (10-Week Experiment)

**Bone marrow myeloid hyperplasia and splenic extramedullary hematopoiesis (EMH).** Bone marrows were hypercellular (Figure 2C), and increased splenic erythroid, myeloid and megakaryocytic EMH (Figure 3B) was observed at all time points post-infection, consistent with inflammation and murine responsive hematopoiesis [35,38]. While erythroid elements were present, bone marrow hypercellularity was primarily due to increased granulopoiesis (myeloid hyperplasia) with increased numbers of blasts (myeloblasts and monoblasts), monocytes and

morphologically benign histiocytes (Figure 2A–B). Increased numbers of blasts in the bone marrow at three weeks post-infection (maturation left shift) were characteristic for accelerated production of granulocytic and/or monocytic precursors in response to ongoing infection (Figure 2B). While differentiating myeloblasts from monoblasts by morphology alone on review of bone marrow cytology is difficult [39], a corresponding increase in blood monocyte counts (Table 2) indicated that a proportion of the blasts were of monocytic origin. Increased granulocytic and monocytic ring forms in bone marrow and blood films (not shown) were consistent with accelerated hematopoiesis in mice [35,39]. These findings correlate with the CBC results of neutrophilia and monocytosis, with ongoing inflammatory disease and neutrophil recruitment to tissues (Table 2; Figure 3A–B), and increased splenic EMH (Figure 3B).

To further evaluate erythropoiesis, enlarged spleens from *Salmonella*-infected mice were analyzed by flow cytometry three weeks after infection. Results from three replicate experiments showed increased numbers of erythroblasts compared to controls

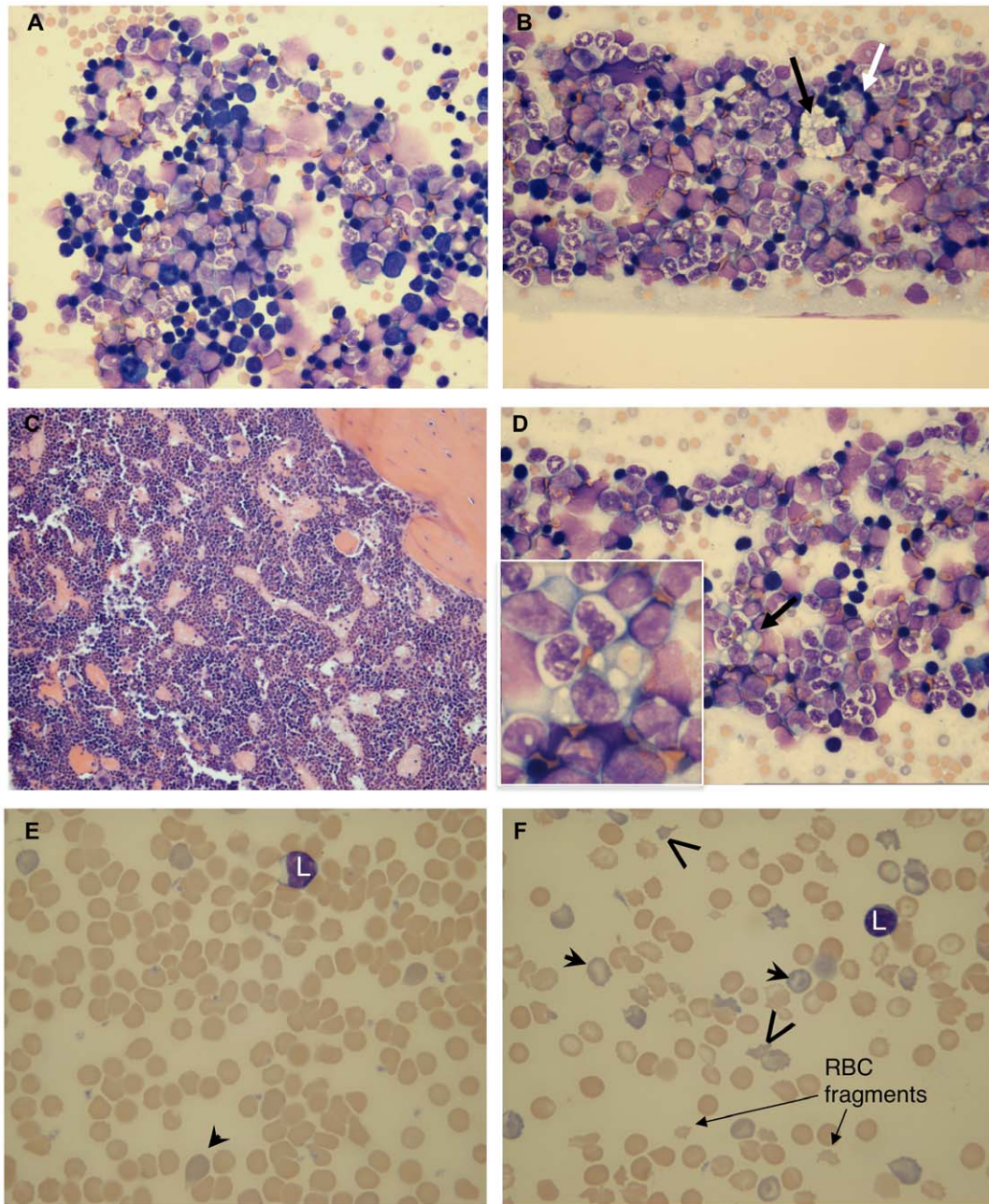


**Figure 2. *S. Typhimurium*-infected mice have increased hemophagocytic macrophages, myeloid hyperplasia, regenerative microcytic anemia and erythrocyte fragmentation.** (A) Control bone marrow cytology, 3 weeks post mock-infection. (B) Infected mouse bone marrow cytology, 3 weeks post-infection; myeloid hyperplasia with increased blasts and monocytes, hemophagocytic macrophage (white arrow), and foamy macrophage (black arrow). (C) Bone marrow histology, 6 weeks post-infection; hypercellularity with myeloid hyperplasia. (D) Mouse bone marrow cytology, 3 weeks post-infection; erythrocyte (arrow and inset) within hemophagocytic macrophage. (E) Control mouse blood film, 3 weeks post mock-infection. (F) Blood film from highly infected mouse, 3 weeks post-infection; marked erythrocyte anisocytosis, increased polychromasia and markedly fragmented erythrocytes (mature and polychromatophilic). Polychromatophilic erythrocytes (arrow-heads), fragmented polychromatophilic erythrocytes (carats), fragmented erythrocytes (arrows), L=small lymphocyte. Wright stain (A, B, D, E, F). H & E stain (C). Original magnifications 500× (A–B, D), 200× (C), or 1000× (E–F). doi:10.1371/journal.pone.0009441.g002

as measured by TER119 staining [40] (Figure 3F–G). Thus, increased splenic erythropoiesis was substantiated and quantified by flow cytometric analysis. Bone marrow and splenic pathology in *S. Typhimurium*-infected mice indicated accelerated hematopoiesis in response to active and ongoing inflammatory disease, anemia and thrombocytopenia.

**Bone marrow hemophagocytic macrophages.** Increased numbers of hemophagocytic macrophages in the bone marrow or spleen are consistent with HLH [5] (Table 1). Review of bone marrow films demonstrated increased hemophagocytic macrophages in mice at all time points post-infection (Table 1; Figure 2B,D), from occasional (1–3/slide) to numerous (1/1–2

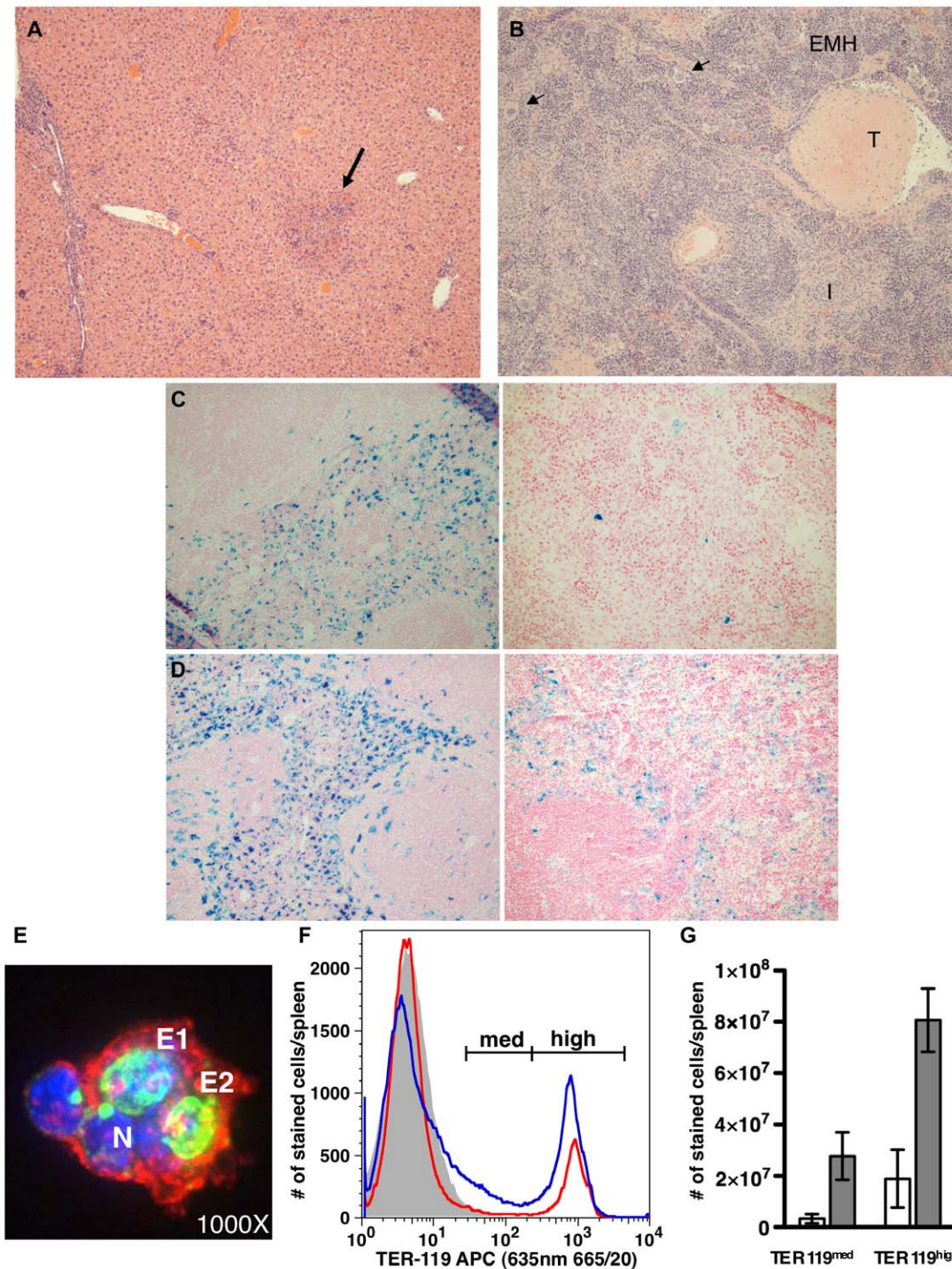


**Figure 3. *S. Typhimurium*-infected mice have tissue inflammation and thrombosis, increased hematopoiesis, and decreased splenic iron.** (A) Mouse liver, 6 weeks post-infection; inflammation and necrosis (arrow). (B) Mouse spleen, 3 weeks post-infection; extramedullary hematopoiesis (EMH; arrow, megakaryocytes), histiocytic infiltration (I) throughout the red pulp, and thrombus (T). H&E stain (A, B). (C) Spleen, mock-infected (left) and infected mouse (right), 3 weeks post-infection; markedly decreased ferric iron staining in red pulp. (D) Spleen, mock-infected (left) and infected mouse (right), 6 weeks post-infection; markedly decreased splenic ferric iron in red pulp. Perl's Prussian Blue stain (C, D). (E) Hemophagocytic macrophage in mouse spleen 3 weeks post-infection that had 10-fold more macrophages and 43-fold more 6N+ macrophages than control mouse spleen. CD11b (red), DAPI (blue), TER119 (green). N = endogenous macrophage nucleus, E1 = nucleated erythrocyte, E2 = non-nucleated erythrocyte. Confocal fluorescent micrograph. (F) Representative histogram overlay of TER119 expression on DAPI+ splenocytes from a mock-infected (red) and infected mouse (blue) 3 weeks post-infection. Filled gray histogram corresponds to the isotype control. The infected mouse had 11.5-fold more TER119<sup>med</sup> pro-erythroblasts and 5.5-fold more TER119<sup>high</sup> erythroblasts than the mock-infected mouse. (G) Mean numbers of TER119<sup>med</sup> and TER119<sup>high</sup> splenocytes from three mock-infected (white bars) and four infected (gray bars) mice. Mean number of TER119<sup>med</sup> pro-erythroblasts per spleen increased 6.8-fold in infected mice, while the mean number of TER119<sup>high</sup> cells, corresponding to all nucleated erythroblasts subsequent to the pro-erythroblast stage [40], increased 3.6-fold. ( $P < 0.05$ ) Error bars = SD. Original magnifications 100× (A–B), 200× (C–D), and 1000× (E). doi:10.1371/journal.pone.0009441.g003

high power field) compared to mock-infected control mice (0–1/slide). Finding two hemophagocytic macrophages per slide is considered significant when reviewing bone marrow cytology for human HLH [28]. Increased hemophagocytosis, present in spleens of infected mice examined by histopathology, was also demonstrated by confocal microscopy via TER119 staining of nucleated and non-nucleated erythrocytes within the cytoplasm of CD11b<sup>high</sup>, GR1<sup>low</sup> macrophages (Figure 3E). Consistent with sHLH and typhoid fever [28,29], *S. Typhimurium*-infected mice have increased numbers of hemophagocytic macrophages in bone marrow and spleen.

**Liver and spleen histopathology, thrombosis and hypofibrinogenemia.** Tissue inflammation and thrombosis occurred in *S. Typhimurium*-infected mice. Acute multifocal to coalescing neutrophilic hepatitis with necrosis was present at one week post-infection. At subsequent time-points, chronic active inflammation was characterized by multifocal to diffuse lymphohistiocytic infiltration with a neutrophilic component, and multifocal areas of hepatocellular necrosis (Figure 3A). Continuous recruitment of neutrophils was evident in all infected mice. Chronic active hepatitis, while not a formalized diagnostic criterion for HLH, is consistent with the described liver lesion in human HLH [5]. Splenic lesions included multifocal histiocytic infiltration and hemophagocytosis, with marked expansion of the red pulp by EMH and morphologically benign histiocytes at all timepoints (Figure 3B). Lymphoid follicular disruption with depletion of the white pulp was also present (Figure 3B), particularly at six and 10 weeks post-infection, consistent with a previously described change in mice with marked EMH in response to anemia [36], and splenic pathology in people with HLH [28]. Hepatic microthrombi were present in two of six mice at one and six weeks post-infection, while marked thrombosis was present in the spleen (Figure 3B) and liver (not shown) in two of six mice at three weeks post-infection. These findings correlated with plasma hypofibrinogenemia in the highly infected mice at three and six weeks post-infection (Table 1). Marked splenic and hepatic thrombosis also occurred in the early death mouse at six weeks post-infection. Masson's staining was negative for fibrosis in liver and spleen sections at all time points (not shown). Thus, persistent hepatosplenomegaly as a result of ongoing inflammatory lesions and EMH in the spleen was present in *S. Typhimurium*-infected mice, and tissue thrombosis correlated with hypofibrinogenemia, an HLH diagnostic criterion [5].

**Hyperferritinemia, hypoferrinemia, decreased tissue iron staining.** Serum iron was decreased at one (two of six mice) and three (four of six mice) weeks (Table 2) post-infection compared to control mice. Hyperferritinemia occurred in 2/6 and 3/10 mice in separate experiments at three weeks post-infection (Table 1). Mice with splenic bacterial loads  $>10^5$  CFU/g and the largest degree of splenomegaly had the most marked hyperferritinemia ( $>4,300$   $\mu\text{g/L}$ ) (Table 1). By six weeks post-infection serum ferritin and iron concentrations were similar to controls although splenomegaly and erythrocyte microcytosis persisted (Tables 1–2). Spleen was the predominant iron storage organ in control mice at all time points where staining intensity for ferric iron in the splenic red pulp (3C–D) was two to four-fold greater than control livers, and four to eight-fold greater than control bone marrows. This is consistent with spleen being the major site for iron storage and EMH [35,33] compared to liver in wild type, healthy mice. Overall, decreased tissue staining for hemosiderin (ferric iron) occurred at all time points post-*S. Typhimurium*-infection in mouse spleen (Figure 3C–D), liver and bone marrow (not shown) compared to mock-infected control

mice. In addition, another feature of HLH, hyperferritinemia, was demonstrated in mice with high tissue bacterial loads, and significant changes in body iron status occurred post-infection with *S. Typhimurium*.

To summarize results, evaluations of blood, bone marrow, liver and spleen of *S. Typhimurium*-infected mice demonstrated active and ongoing hematopoiesis, inflammatory disease, and six of eight characteristics of sHLH in highly infected mice.

## Discussion

Infection of Sv129S6 wild-type mice with *S. Typhimurium* via the natural oral route precipitates, as expected [18,19], an acute inflammatory response followed by subacute to chronic inflammatory disease. While the inflammatory response is consistent with prior descriptions of murine typhoid fever [18,19,23,31], new to this infectious disease model are clinico-pathologic features of HLH (Table 1) demonstrated by increased hemophagocytic macrophages in bone marrow and spleen, fever, hepatosplenomegaly, bi-cytopenia (anemia, thrombocytopenia), hypofibrinogenemia, and hyperferritinemia ( $>1400$   $\mu\text{g/L}$ ). At three weeks post-infection, the most severely infected mice with the highest bacterial CFU/g of spleen meet six of eight of the HLH diagnostic criteria, five of which are needed to diagnose HLH in humans [5]. These data substantiate a novel clinical mouse model for sHLH.

While a diagnosis of HLH cannot be solely based on finding hemophagocytic macrophages, an increased number especially in bone marrow cytology (Figures 2B,D) and spleen (Figure 3E) is a classic characteristic of HLH [5,28], and also occurs with human typhoid fever [3,28,29]. In a prior study demonstrating hemophagocytic macrophages in livers of infected mice, *S. Typhimurium* was shown to survive and replicate in tissue culture hemophagocytic macrophages [24]. Erythrophagocytic macrophages have been shown to express heme-oxygenase 1 (HO-1) in human sepsis cases [41], and inhibit pro-inflammatory cytokine production in cultured mouse bone marrow cells (Slc11a1/Nramp1<sup>+/+</sup>) [42], thereby suggesting an anti-inflammatory role. Increased serum HO-1 also occurs in cases of sHLH in correlation with hyperferritinemia [43]. Whether HO-1 facilitates *S. Typhimurium* survival in hemophagocytic macrophages is unknown, however, a plausible hypothesis is that intracellular bacterial access to iron released during heme breakdown following erythrophagocytosis provides *S. Typhimurium* with an essential survival nutrient. Thus, hemophagocytic macrophages may provide a survival niche for *S. Typhimurium* contributing to the subclinical chronic carrier state important in people and mice with typhoid fever, as well as the pathology of cytopenias, including anemia and thrombocytopenia, in *Salmonella*-infected mice. Hemophagocytic macrophages may have an anti-inflammatory effect, provide *S. Typhimurium* a survival niche, and contribute to development of cytopenias, all of which could help elucidate mechanisms of sHLH disease pathogenesis in this natural infectious disease model.

Activated macrophages are integral to the development of HLH [1,2]. Secretion of plasminogen activator by activated macrophages contributes to the coagulopathies that occur in HLH [2,28]. Indeed, disseminated intravascular coagulation (DIC) has been reported in humans with HLH [1,3,44] or typhoid fever [45], and highly infected mice in our study had characteristics of DIC including thrombocytopenia, (Figure 1; Tables 1–2) hypofibrinogenemia, tissue thrombosis (Figure 3B), and schistocytes in the blood (Figure 2F). In humans, severe hyperferritinemia in HLH correlates with death [1] and is useful as a diagnostic marker for HLH [4,5,43,44]. Serum ferritin levels are highest ( $>12,000$   $\mu\text{g/L}$ ) in human histiocytic disorders in which the patients also have

DIC [44]. Approximately 30% of *S. Typhimurium*-infected mice in our studies had hyperferritinemia that was greatest ( $>4,300 \mu\text{g/L}$ ) in mice with most severe splenomegaly and splenic bacterial CFU (Table 1). Hyperferritinemia has also been reported in canine and feline histiocytic disorders [6,9], and in acute *S. Typhimurium* infection in mice [23], and should alert both human and veterinary clinicians to the possibility of hemophagocytic histiocytic disorders. These observations collectively indicate activated macrophages play a key role in the pathophysiology of *S. Typhimurium*-induced sHLH.

The pathogenesis of bi-cytopenia in this mouse model is likely multifactorial. Adequate to increased megakaryocytes in bone marrow (Figure 2C) and spleen (Figure 3B) make lack of platelet production an unlikely cause for thrombocytopenia. Platelet sequestration within enlarged spleens may have contributed to thrombocytopenia. Additionally, increased platelet destruction by hemophagocytosis or platelet consumption from DIC [35] may have occurred in highly infected mice (Table 1). Also, regardless of bacterial tissue load, *S. Typhimurium*-infected mice developed erythrocyte microcytosis, and highly infected mice developed a regenerative microcytic anemia that differed from ACD by a demonstrated lack of tissue iron sequestration [35,46] (Figure 3C–D) even in mice with hyperferritinemia. Our findings of increased erythropoiesis and hemophagocytosis differ from the non-regenerative anemia previously described in acute, fatal *S. Typhimurium* infection in genetically susceptible mouse strains [23]. The pathogenesis of microcytosis in *S. Typhimurium*-infected mice in our studies may involve several mechanisms including iron deficiency [37,47] or fragmentation of erythrocytes [48] known to occur with both iron deficiency [37] and DIC. Erythrocyte fragmentation was severe enough to decrease MCV only in highly infected mice that also had evidence of DIC and low serum iron concentration. Persistent microcytosis following recovery of anemia and reduced tissue iron staining indicate iron stores were mobilized to support erythropoiesis and/or sequestered in ferritin as a result of increased heme breakdown by macrophages. As iron stores were depleted, ongoing accelerated erythropoiesis could have resulted in a progressive decrease in MCV as in iron deficiency. Another hypothesis for persistent microcytosis is altered iron metabolism. Changes in iron metabolism have been demonstrated in response to acute *S. Typhimurium* infections in susceptible strains of mice [23] and in tissue culture macrophages [49]. Functional iron deficiency may be a mechanism for controlling infection by limiting microbial access to iron. Decreased intracellular iron content of *S. Typhimurium*-infected macrophages [49] is consistent with reduced tissue iron storage in macrophages (Figure 3C–D) and differs from ACD. These findings suggest iron was mobilized from tissues to support stimulated erythropoiesis in the face of cytopenias, because of increased ferritin synthesis, and alternatively, or in addition, there may have been efflux of iron from macrophages presumably via the iron exporter ferroportin to reduce intracellular *S. Typhimurium* access to iron, a mechanism previously described [49]. Thus, the hematologic effects and depleted tissue iron storage in chronic *S. Typhimurium*-infected mice differentiate it from ACD and from acute fatal murine salmonellosis, and this model provides an opportunity to study mechanisms for anemia in HLH and altered iron trafficking in response to infection with *S. Typhimurium*.

The mouse strain chosen for this study was important given the effect of murine genetic variability on iron homeostasis [50], hematology [23,35,38] and *S. Typhimurium* resistance [19,22]. Sv129S6 mice, intact for *Slc11a1/Nramp1* which helps maintain iron homeostasis via phagolysosomal transport of divalent cations including iron [49], efficiently recycle erythrocyte-derived iron in

macrophages [51], and are resistant to *S. Typhimurium* infection [19]. Indeed iron loading has been shown to increase susceptibility to acute *S. Typhimurium* infection in mice [23], therefore, iron deficiency may have contributed to increased bacterial resistance in our studies. In addition, Sv129 mice are better able to maintain iron homeostasis under conditions of both iron deficiency and excess compared to other mouse strains including C57BL/6, DBA/2 and CBA [50]. Wild type Sv129S6 mice have been shown to mobilize liver iron stores in response to iron deficiency where iron-limited erythropoiesis was maintained in the face of developing microcytosis [47]. Therefore, this Sv129S6 infection model may prove particularly useful in elucidating mechanisms of anemia in HLH, and altered iron homeostasis and anemia during chronic *S. Typhimurium* infection that are different from ACD.

Due to expansion of red pulp by EMH and inflammation, splenomegaly persists in mice even after bacterial CFU have cleared. Persistent splenomegaly also occurs in human HLH [2], and in prior studies of *S. Typhimurium*-infected mice [19,31]. This mechanism may include persistence of bacterial antigen, for instance on follicular dendritic cells and/or on MHC class II molecules [22,52,53], that continues to drive cytokine production, inflammation and increased EMH in response to anemia and thrombocytopenia, resulting in persistent splenomegaly. Importantly, mice with the greatest magnitude of splenomegaly also had the most severe cytopenias.

Approximately 30% of the mice in our studies developed clinical neurological signs from which most recovered. The incidence of neurological disease in HLH patients varies from 37% in children [34], to 7–47% for all patients [3]. Neurological disease, while previously characterized in *Slc11a1/Nramp1* wild type mice orally infected with *S. Typhimurium* [32], is clearly relevant to both HLH and typhoid fever, and may provide a means to clinically monitor response to therapeutic interventions.

Abnormal lipid processing is known to occur with HLH [5,28,54], and one of the diagnostic criteria for HLH is hypertriglyceridemia [5]. An effect on lipid processing in *S. Typhimurium*-infected mice is suspected based on finding vacuolated lymphocytes on blood films and foamy bone marrow macrophages (Figure 2B), features that also occur with lipid storage diseases [55,56]. Cytokine-mediated decreases in lipoprotein lipase have been shown to occur with increased  $\text{IFN}\gamma$  and  $\text{TNF}\alpha$  in mice [57], and  $\text{TNF}\alpha$  in human tHLH patients [54]. In addition, a role for lipid (via cholesterol esterification) in intracellular survival of *S. Typhimurium* has been suggested [58]. A future direction for understanding HLH pathophysiology in this model will be investigating altered lipid metabolism including lipoprotein lipase, triglycerides, cholesterol and  $\text{PGF}2\alpha$  analyses.

The important findings in highly infected mice in this chronic systemic infection model are those demonstrating first, an HLH syndrome and second, anemia different from ACD and acute murine *S. Typhimurium* infection. To understand how HLH develops and can be ameliorated, it is necessary to understand the molecular and cellular events that can precipitate HLH. A viable animal model is critical to understanding pathogenesis and for intervention strategies. Thus, future directions for this mouse model include cytokine profiling and characterization of specific lipid and iron cellular markers and metabolism. A further understanding of the unique pathologies of increased hemophagocytosis, hyperferritinemia and inflammatory disease without tissue iron loading, in the face of microcytic anemia may help elucidate pathophysiology of anemia in HLH that differs from ACD. Features of *S. Typhimurium*-infected mice that substantiate its value as an sHLH animal model include a natural host-pathogen interaction, no known single-locus genetic component,

death is not the endpoint, a commercially available mouse strain and infectious agent, and a tissue-load dependent and manipulable model. *S. Typhimurium*-infected mice have the features of sHLH yet have a low mortality rate (approximately 7%) even without treatment intervention. This provides a viable model to study sHLH pathogenesis over time, and novel targets for HLH therapies and therapeutic response by clinical, hematological, immunological, pathological and molecular means.

## Materials and Methods

### Ethics Statement

Research protocols were in accordance with the NIH Guide for the Care and Use of Laboratory Animals, and approved by the University of Colorado Institutional Biosafety and Animal Care and Use Committees.

To characterize hematological responses and establish clinicopathologic features of HLH in *S. Typhimurium*-infected mice, two studies of 16 and 10 weeks duration, respectively, were undertaken. Specific HLH diagnostic criteria [5] analyzed included hemophagocytic macrophages in bone marrow and spleen, fever, splenomegaly, cytopenias, plasma fibrinogen, and serum ferritin.

### Bacteria and Mice

Freshly struck colonies of virulent *Salmonella enterica* serotype Typhimurium strain SL1344 (StrR) [24,59], inoculated into Luria-Bertani broth were grown at 37°C with aeration overnight. Bacteria were pelleted and resuspended in sterile PBS at  $9.1 \times 10^8 - 2.0 \times 10^9$  CFU in 100  $\mu$ L, as determined by plating. Streptomycin (200  $\mu$ g/mL) was added to media to select for *S. Typhimurium*. Female seven week-old Sv129S6/SvEvTac mice (Taconic Farms, Inc.; Hudson, NY) were fasted for 12–16 hours prior to infection, and housed separately from mock-infected control mice.

### 16-Week Experiment

**Hematology and IgG enzyme-linked immunosorbent assay (ELISA).** Blood (50–150  $\mu$ L) was collected bi-weekly by retro-orbital method into Microvette K<sub>2</sub>-EDTA tubes (Sarstedt, Inc; Newton, NC) for CBC using a Hemavet HV950FS analyzer (Drew Scientific; Waterbury, CT). Simultaneously, serum was collected from one mock-infected control and five infected mice for IgG to *Salmonella* O-Antigen analysis. Following euthanasia, whole spleen, liver, and MLN were weighed, homogenized and plated for bacterial CFU. Serum IgG to *Salmonella* O-Antigen, measured by anti-*Salmonella* IgG ELISA included an overnight culture of *S. Typhimurium* that was pelleted, washed with PBS, weighed and sonicated in PBS. Supernatant was harvested after one hour centrifugation at 4,000 g and diluted to 100 ng of bacteria per 100  $\mu$ L. 100  $\mu$ L of lysate was incubated overnight in 96-well ELISA plates (Nunc; Rochester, NY). Coated wells were washed and blocked (PBS with 0.05% Tween, 1% Bovine Serum Albumin) for one hr at 37°C. Sera were diluted serially in blocking buffer, incubated in blocked wells for two hours at room temperature, then washed. Anti-mouse IgG antibody conjugated to horseradish peroxidase (HRP) (Abcam ab6728-1; Cambridge, MA) was added (1:4000), incubated for two hours at room temperature, washed and incubated with HRP substrate according to instructions (Pierce Protein Research Products, Rockford, IL). Absorbance was read at 450 nm with a plate reader. Serum titer was determined from the highest dilution of serum to give an optical density above pre-immune serum background.

### 10-Week Experiment

**Body temperature and blood collection.** The submandibular vascular bundle collection method replaced retro-orbital bleeding to minimize distress to the animal and allow for greater collection volume [60]. Approximately 300  $\mu$ L of blood was collected into Microtainer K<sub>2</sub>-EDTA and serum tubes (BD; Franklin Lakes, NJ) for hematology and serum analyses at a single time-point in mice which were then euthanized at one, three, six and ten weeks post-infection. Blood kept at room temperature was analyzed within four hours of collection for all parameters except ferritin, which was frozen for later analysis. Complete blood counts were performed using mouse specific instrumentation on an ADVIA 120 hematology analyzer with Multispecies software (version 3.1.8.0-MS) (Bayer Corporation, Tarrytown, NY). Serum iron was measured with an Hitachi 917 analyzer (Roche Diagnostics, Indianapolis, IN). Plasma fibrinogen was measured by heat precipitation method. Fresh blood smears were Wright-stained, and manual leukocyte differential counts were performed to address increased percentages of large unstained cells (LUC) measured by the Advia 120 in seventeen of twenty infected mice (range 2.0–6.0%) compared to mock-infected controls (mean 1.0%). The majority of LUC (1–4%) were activated monocytes, the remainder were large lymphocytes; automated monocyte counts were corrected accordingly. Neurological signs and body temperatures were recorded at the same time daily, and body weights weekly. Five temperature measurements per mouse were made daily by digital infrared thermometer (MT-100; Micro Temp, Troy, MI) as previously described [61]. Mean difference between infected and mock-infected mice for each day was computed and tested in a one-sided paired *t* test to establish whether the difference was greater than zero.  $P < 0.05$  was considered significant (GAUSS Mathematical & Statistical System Version 8.0; Aptech Systems, Inc.; Black Diamond, WA).

**Cyto- and histopathology.** Following euthanasia whole spleen and liver were weighed; a section of each was weighed, homogenized and plated for bacterial CFU. No CFU were found in any mock-infected animals. Remaining liver and spleen, and one femur were collected into 10% neutral buffered formalin for histological evaluation. Bone marrow brush smear preparations were made immediately post-mortem from the second femur, and Wright-stained for cytological examination. Tissues were processed by routine histological methods; paraffin sections were stained with hematoxylin and eosin (H & E), Perl's Prussian blue for ferric iron (hemosiderin), and Masson's trichrome stain for fibrosis [62]. Intensity of iron tissue staining was subjectively scored on a scale of 0 – 4+ by light microscopy. Photomicrographs were taken with an Olympus BX50 (Olympus Corporation, Center Valley, PA) using NIS-Elements package F3.0 Nikon Laboratory Imaging software (Nikon Corporation, Tokyo, Japan).

**Serum ferritin ELISA.** Ferritin was quantified using a commercially available mouse ELISA kit (E-90F, Immunology Consultants Laboratory, Inc; Newberg, OR). Absorbance at 450 nm was determined with a plate reader; ferritin concentrations were calculated based on standard curves developed within the same plate and corrected for sample dilution. To verify findings, serum ferritin was measured in duplicated infection experiments using an additional 10 *S. Typhimurium*-infected and three mock-infected control mice at three weeks post-infection.

**Flow cytometry and cell sorting.** Spleens from mice collected three weeks after *S. Typhimurium* infection were mechanically homogenized and passed through a 70  $\mu$ m cell strainer (BD Biosciences, San Jose, CA) to obtain single cell suspensions. Non-nucleated erythrocytes were lysed in hypotonic

buffer containing 0.16 M NH<sub>4</sub>Cl, 10 mM KHCO<sub>3</sub> and 0.1 mM EDTA. Non-lysed cells were passed through a 40 μm cell strainer and re-suspended in staining buffer (PBS +1% FBS and 0.02% sodium azide) containing anti-mouse CD16/32 (eBioscience, San Diego, CA) to block Fc receptors. For analysis of erythroblasts, cells were then stained with allophycocyanin-conjugated anti-mouse TER119 antibody [40] (BD Biosciences, San Jose, CA), followed by staining for DNA in 10 μg/mL DAPI (Invitrogen, Carlsbad, CA). Fluorescently labeled cells were quantified using a CyAn ADP flow cytometer (Beckman Coulter, Fullerton, CA) and analyzed using FlowJo software (Tree Star, Inc., Ashland, Or). For hemophagocytic macrophage sorting, cells were stained with phycoerythrin-conjugated anti-mouse CD11b and fluorescein isothiocyanate-conjugated anti-mouse GR1 antibodies (eBioscience, San Diego, CA). Splenocytes were fixed in 1% paraformaldehyde/1% sucrose and permeabilized in 0.1% saponin, then stained intracellularly for erythrocytes with allophycocyanin-conjugated anti-mouse TER119 antibody, followed by staining for DNA in 10 μg/ml DAPI. Cells were passed through another 40 μm cell strainer, then sorted for CD11b<sup>high</sup>, GR1<sup>low</sup> macrophages with at least 6N DNA content using a MoFloXDP cell sorter (Beckman Coulter, Fullerton, CA), and cytopun onto poly-L-lysine coated slides (Wescor, Logan, UT) for

microscopic analysis. Confocal fluorescent micrographs were captured using a Yokogawa CSU10 spinning disk confocal (Tokyo, Japan) on a Nikon Eclipse TE2000-U inverted microscope (Tokyo, Japan) with a 100× Plan Apo numerical aperture 1.4 objective lens, and acquired with a Cascade II:512 (Photometrics, Tucson, AZ) camera using MetaMorph 7.0 software (Molecular Devices, Sunnyvale, CA).

**Statistics.** Mann-Whitney U Test and Student's *t*-Test were performed and considered significant at *P*<0.05. Results from both tests were similar; only *t*-Test results are shown.

### Acknowledgments

The authors acknowledge Elizabeth Chlipala, Premier Laboratory, for expert advice and use of the Hemavet 950 analyzer; Dr. Linda Vap and Staff, Colorado State University, for expert advice and use of the Advia 120 hematology analyzer; Todd Bass and Staff, Colorado State University, for expert advice and histochemistry.

### Author Contributions

Conceived and designed the experiments: DEB MWM MCP RNN CSD. Performed the experiments: DEB MWM MCP RNN CSD. Analyzed the data: DEB MWM MCP RNN CSD. Wrote the paper: DEB CSD.

### References

- Créput C, Galicier L, Buyse S, Azoulay E (2008) Understanding organ dysfunction in hemophagocytic lymphohistiocytosis. *Intensive Care Med* 34: 1177–1187.
- Janka GE (2007) Hemophagocytic syndromes. *Blood Rev* 21: 245–253.
- Fisman DN (2000) Hemophagocytic syndromes and infection. *Emerging Infect Dis* 6: 601–608.
- Allen CE, Yu X, Kozinetz CA, McClain KL (2008) Highly elevated ferritin levels and the diagnosis of hemophagocytic lymphohistiocytosis. *Pediatr Blood Cancer* 50: 1227–1235.
- Henter J, Horne A, Aricó M, Egeler R, Filipovich A, et al. (2007) HLH-2004: Diagnostic and therapeutic guidelines for hemophagocytic lymphohistiocytosis. *Pediatr Blood Cancer* 48: 124–131.
- Newlands CE, Houston DM, Vasconcelos DY (1994) Hyperferritinemia associated with malignant histiocytosis in a dog. *J Am Vet Med Assoc* 205: 849–851.
- Moore PF, Affolter VK, Vernau W (2006) Canine hemophagocytic histiocytic sarcoma: a proliferative disorder of CD11d+ macrophages. *Vet Pathol* 43: 632–645.
- Weiss DJ (2007) Hemophagocytic syndrome in dogs: 24 cases (1996–2005). *J Am Vet Med Assoc* 230: 697–701.
- Friedrichs KR, Young KM (2008) Histiocytic sarcoma of macrophage origin in a cat: case report with a literature review of feline histiocytic malignancies and comparison with canine hemophagocytic histiocytic sarcoma. *Vet Clin Pathol* 37: 121–128.
- Spangler WL, Kass PH (1999) Splenic myeloid metaplasia, histiocytosis, and hypersplenism in the dog (65 cases). *Vet Pathol* 36: 583–593.
- Henter JI, Ehrnst A, Andersson J, Elinder G (1993) Familial hemophagocytic lymphohistiocytosis and viral infections. *Acta Paediatr* 82: 369–372.
- Jordan MB, Hildeman D, Kappler J, Marrack P (2004) An animal model of hemophagocytic lymphohistiocytosis (HLH): CD8+ T cells and interferon gamma are essential for the disorder. *Blood* 104: 735–743.
- Crozat K, Hoebe K, Ugolini S, Hong N, Janssen E, et al. (2007) Jinx, an MCMV susceptibility phenotype caused by disruption of Unc13d: a mouse model of type 3 familial hemophagocytic lymphohistiocytosis. *J Exp Med* 204: 853–863.
- Schmid JP, Ho C, Diana J, Pivert G, Lehuen A, et al. (2008) A Griscelli syndrome type 2 murine model of hemophagocytic lymphohistiocytosis (HLH). *European Journal of Immunology* 38: 3219–3225.
- Chan C, Abe M, Hashimoto N, Hao C, Williams I, et al. (2009) Mice lacking asparaginyl endopeptidase develop disorders resembling hemophagocytic syndrome. *Proc Natl Acad Sci U S A* 106: 468–473.
- Castillo L, Castillo J (2009) Secondary hemophagocytic lymphohistiocytosis and severe sepsis/systemic inflammatory response syndrome/multiorgan dysfunction syndrome/macrophage activation syndrome share common intermediate phenotypes on a spectrum of inflammation. *Pediatr Crit Care Med* 10: 387–392.
- Nahum E, Ben-Ari J, Stain J, Schonfeld T (2000) Hemophagocytic lymphohistiocytic syndrome: Unrecognized cause of multiple organ failure. *Pediatr Crit Care Med* 1: 51–54.
- Santos RL, Zhang S, Tsois RM, Kingsley RA, Adams LG, et al. (2001) Animal models of Salmonella infections: enteritis versus typhoid fever. *Microbes Infect* 3: 1335–1344.
- Monack DM, Bouley DM, Falkow S (2004) Salmonella typhimurium persists within macrophages in the mesenteric lymph nodes of chronically infected Nrampl1+/+ mice and can be reactivated by IFNγ neutralization. *J Exp Med* 199: 231–241.
- Vazquez-Torres A, Jones-Carson J, Bäuml AJ, Falkow S, Valdivia R, et al. (1999) Extraintestinal dissemination of Salmonella by CD18-expressing phagocytes. *Nature* 401: 804–808.
- Tsois RM, Kingsley RA, Townsend SM, Ficht TA, Adams LG, et al. (1999) Of mice, calves, and men. Comparison of the mouse typhoid model with other Salmonella infections. *Adv Exp Med Biol* 473: 261–274.
- Roy M, Malo D (2002) Genetic regulation of host responses to Salmonella infection in mice. *Genes Immun* 3: 381–393.
- Roy M, Riendeau N, Bedard C, Helie P, Gundula M, et al. (2007) Pyruvate kinase deficiency confers susceptibility to Salmonella typhimurium infection in mice. *J Exp Med* 204: 2949–2961.
- Nix RN, Altschuler SE, Henson PM, Detweiler CS (2007) Hemophagocytic macrophages harbor Salmonella enterica during persistent infection. *PLoS Pathog* 3: e193.
- Richter-Dahlfors A, Buchan AM, Finlay BB (1997) Murine salmonellosis studied by confocal microscopy: Salmonella typhimurium resides intracellularly inside macrophages and exerts a cytotoxic effect on phagocytes in vivo. *J Exp Med* 186: 569–580.
- Fink SL, Cookson BT (2007) Pyroptosis and host cell death responses during Salmonella infection. *Cell Microbiol* 9: 2562–2570.
- Shin BM, Paik IK, Cho HI (1994) Bone marrow pathology of culture proven typhoid fever. *J Korean Med Sci* 9: 57–63.
- Favara BE (1992) Hemophagocytic lymphohistiocytosis: a hemophagocytic syndrome. *Semin Diagn Pathol* 9: 63–74.
- Singh ZN, Rakhjea D, Yadav TP, Shome DK (2005) Infection-associated haemophagocytosis: the tropical spectrum. *Clin Lab Haem* 27: 312–315.
- Veerakul G, Sanpakit K, Tanphaichitr V, Mahasandana C, Jirarattanasopa N (2002) Secondary hemophagocytic lymphohistiocytosis in children: an analysis of etiology and outcome. *J Med Assoc Thai* 85: S530–541.
- Johansson C, Ingman M, Jo Wick M (2006) Elevated neutrophil, macrophage and dendritic cell numbers characterize immune cell populations in mice chronically infected with Salmonella. *Microb Pathog* 41: 49–58.
- Wickham ME, Brown NF, Provias J, Finlay BB, Coombes BK (2007) Oral infection of mice with Salmonella enterica serovar Typhimurium causes meningitis and infection of the brain. *BMC Infect Dis* 7: 65.
- Percy DH, Barthold SW (2007) Mouse. In: Percy DH, Barthold SW, eds. *Pathology of Laboratory Rodents and Rabbits*. Ames, IA: Blackwell Pub. pp 3–124.
- Horne A, Trottestam H, Aricó M, Egeler R, Filipovich A, et al. (2008) Frequency and spectrum of central nervous system involvement in 193 children with haemophagocytic lymphohistiocytosis. *Br J Haematol* 140: 327–335.
- Everds N (2007) Hematology of the laboratory mouse. In: Fox JG, Barthold SW, Davison MT, Newcomer CE, Quimby FW, Smith AL, eds. *The Mouse in*

- Biomedical Research, 2nd ed. Vol 3. San Diego, CA: Academic Press. pp 133–170.
36. Ohgami RS, Campagna DR, Antiochos B, Wood E, Sharp J, et al. (2005) nm1054: a spontaneous, recessive, hypochromic, microcytic anemia mutation in the mouse. *Blood* 106: 3625–3631.
  37. Burkhard M, Brown D, McGrath J, Meador V, Mayle D, et al. (2001) Evaluation of the erythroid regenerative response in two different models of experimentally induced iron deficiency anemia. *Vet Clin Pathol* 30: 76–85.
  38. Car BD, Eng VM (2001) Special considerations in the evaluation of the hematology and hemostasis of mutant mice. *Vet Pathol* 38: 20–30.
  39. Biermann H, Pietz B, Dreier R, Schmid KW, Sorg C, et al. (1999) Murine leukocytes with ring-shaped nuclei include granulocytes, monocytes, and their precursors. *J Leukoc Biol* 65: 217–231.
  40. Socolovsky M, Nam H, Fleming MD, Haase VH, Brugnara C, et al. (2001) Ineffective erythropoiesis in Stat5a(-/-)5b(-/-) mice due to decreased survival of early erythroblasts. *Blood* 98: 3261–3273.
  41. Schaer DJ, Schaer CA, Schoedon G, Imhof A, Kurrer MO (2006) Hemophagocytic macrophages constitute a major compartment of heme oxygenase expression in sepsis. *Eur J Haematol* 77: 432–436.
  42. Delaby C, Pilard N, Hetet G, Driss F, Grandchamp B, et al. (2005) A physiological model to study iron recycling in macrophages. *Exp Cell Res* 310: 43–53.
  43. Kirino Y, Takeno M, Iwasaki M, Ueda A, Ohno S, et al. (2005) Increased serum HO-1 in hemophagocytic syndrome and adult-onset Still's disease: use in the differential diagnosis of hyperferritinemia. *Arthritis Res Ther* 7: R616–624.
  44. Esumi N, Ikushima S, Hibi S, Todo S, Imashuku S (1988) High serum ferritin level as a marker of malignant histiocytosis and virus-associated hemophagocytic syndrome. *Cancer* 61: 2071–2076.
  45. Spencer DC, Pienaar NL, Atkinson PM (1988) Disturbances of blood coagulation associated with *Salmonella typhi* infections. *J Infect* 16: 153–161.
  46. Weiss G (2009) Iron metabolism in the anemia of chronic disease. *Biochim Biophys Acta* 1790: 682–693.
  47. Ajioka RS, Levy JE, Andrews NC, Kushner JP (2002) Regulation of iron absorption in Hfe mutant mice. *Blood* 100: 1465–1469.
  48. Bessman D (1978) Microcytosis caused by RBC fragmentation. Confirmation by RBC size distribution analysis. *JAMA* 239: 2475–2476.
  49. Nairz M, Theurl I, Ludwiczek S, Theurl M, Mair S, et al. (2007) The coordinated regulation of iron homeostasis in murine macrophages limits the availability of iron for intracellular *Salmonella typhimurium*. *Cell Microbiol* 9: 2126–2140.
  50. Dupic F, Fruchon S, Bensaid M, Loreal O, Brissot P, et al. (2002) Duodenal mRNA expression of iron related genes in response to iron loading and iron deficiency in four strains of mice. *Gut* 51: 648–653.
  51. Soe-Lin S, Apte SS, Andriopoulos B, Andrews M, Schranzhofer M, et al. (2009) Nramp1 promotes efficient macrophage recycling of iron following erythrophagocytosis in vivo. *Proc Natl Acad Sci U S A* 106: 5960–5965.
  52. Nauciel C, Ronco E, Guenet JL, Pla M (1988) Role of H-2 and non-H-2 genes in control of bacterial clearance from the spleen in *Salmonella typhimurium*-infected mice. *Infect Immun* 56: 2407–2411.
  53. Hormaeche CE, Harrington KA, Joysey HS (1985) Natural resistance to salmonellae in mice: control by genes within the major histocompatibility complex. *J Infect Dis* 152: 1050–1056.
  54. Henter JI, Carlson LA, Söder O, Nilsson-Ehle P, Elinder G (1991) Lipoprotein alterations and plasma lipoprotein lipase reduction in familial hemophagocytic lymphohistiocytosis. *Acta Paediatr Scand* 80: 675–681.
  55. Anderson G, Smith VV, Malone M, Sebire NJ (2005) Blood film examination for vacuolated lymphocytes in the diagnosis of metabolic disorders; retrospective experience of more than 2,500 cases from a single centre. *J Clin Pathol* 58: 1305–1310.
  56. Brown DE, Thrall MA, Walkley SU, Wenger D, Mitchell T, et al. (1994) Feline Niemann-Pick disease type C. *Am J Pathol* 144: 1412–1415.
  57. Feingold KR, Marshall M, Gulli R, Moser AH, Grunfeld C (1994) Effect of endotoxin and cytokines on lipoprotein lipase activity in mice. *Arterioscler Thromb* 14: 1866–1872.
  58. Nawabi P, Catron DM, Haldar K (2008) Esterification of cholesterol by a type III secretion effector during intracellular *Salmonella* infection. *Mol Microbiol* 68: 173–185.
  59. Smith BP, Reina-Guerra M, Hoiseth SK, Stocker BA, Habasha F, et al. (1984) Aromatic-dependent *Salmonella typhimurium* as modified live vaccines for calves. *Am J Vet Res* 45: 59–66.
  60. Golde WT, Gollobin P, Rodriguez LL (2005) A rapid, simple, and humane method for submandibular bleeding of mice using a lancet. *Lab Anim (NY)* 34: 39–43.
  61. Saegusa Y, Tabata H (2003) Usefulness of infrared thermometry in determining body temperature in mice. *J Vet Med Sci* 65: 1365–1367.
  62. Prophet E, Mills B, Arrington JB, Sobin LH (1992) *Laboratory Methods in Histotechnology*. Washington, DC: Armed Forces Institute of Pathology (US). American Registry of Pathology. 254 p.